

1 GRIDSS2: comprehensive 2 characterisation of somatic structural 3 variation using single breakend variants 4 and structural variant phasing

5 Daniel L. Cameron^{1,2,3}, Jonathan Baber^{3,4}, Charles Shale^{3,4}, Jose
6 Espejo Valle-Inclan⁵, Nicolle Besselink⁵, Arne van Hoeck⁵, Roel
7 Janssen⁵, Edwin Cuppen^{4,5}, Peter Priestley^{3,4}, Anthony T.
8 Papenfuss^{1,2,6,7}

9 ¹ Bioinformatics Division, Walter and Eliza Hall Institute of Medical Research, Parkville, Australia

10 ² Department of Medical Biology, University of Melbourne, Australia

11 ³ Hartwig Medical Foundation Australia, Sydney, Australia

12 ⁴ Hartwig Medical Foundation, Science Park 408, Amsterdam, The Netherlands

13 ⁵ Center for Molecular Medicine and Oncode Institute, University Medical Center Utrecht,
14 Heidelberglaan 100, Utrecht, The Netherlands

15 ⁶ Peter MacCallum Cancer Centre, Melbourne, Australia

16 ⁷ Sir Peter MacCallum Department of Oncology, University of Melbourne, Australia

17

18 Correspondence: Daniel L. Cameron (cameron.d@wehi.edu.au) and Anthony T. Papenfuss
19 (papenfuss@wehi.edu.au)

20

21 Abstract

22 GRIDSS2 is the first structural variant caller to explicitly report single breakends - breakpoints in
23 which only one side can be unambiguously determined. By treating single breakends as a
24 fundamental genomic rearrangement signal on par with breakpoints, GRIDSS2 can explain 47%
25 of somatic centromeric copy number changes using single breakends to non-centromeric
26 sequence, with chromosome 1 exhibiting a unique centromeric rearrangement signature. On a
27 cohort of 3,782 deeply sequenced metastatic cancers, GRIDSS2 achieved an unprecedented
28 3.1% false negative rate and identified a novel 32-100bp duplication signature. Somatic
29 structural variants are highly clustered with GRIDSS2 phasing 16% using just paired-end
30 sequencing.

31 Keywords

32 Single breakends, somatic, structural variation

33 Background

34 The reliable detection of structural variants (SVs) is critical to understanding the role genome
35 architecture plays in health and disease. This is especially important in cancer and precision
36 medicine where structural variation can be a key driver mutation ^{1,2}. Over the past decade,
37 many tools have been developed for the detection of genomic rearrangements, which have
38 been the subject of recent extensive benchmarks ^{3,4}. These tools fall broadly into two camps:
39 those that detect changes in DNA abundance, known as copy number variant or aberration
40 (CNV/CNA) callers, and those that detect non-reference DNA adjacencies, known as structural
41 variant (SV) or breakpoint callers. While CNAs and SVs are merely two different viewpoints of
42 the underlying genomic rearrangements, the methods of detection are fundamentally different.

43 Here, we address the problem of SV detection and show that breakpoint detection alone is
44 insufficient for the comprehensive characterisation of somatic genomic rearrangements that
45 occur in cancer. A third genomic rearrangement primitive is essential: single breakends.

46 The Variant Call Format (VCF)⁵ defines a single breakend as a breakpoint in which only one
47 side can be unambiguously placed. This can occur due to one of two reasons. Firstly, the
48 sequence on one side of the breakpoint could be absent from the reference. Either non-
49 reference sequence could be present due to the integration of foreign DNA (e.g. provirus) or the
50 reference could lack sequence present in the sample. Secondly, breakpoints into highly
51 repetitive regions cannot be unambiguously placed. Single breakends allow the representation
52 of such breakpoints. Such rearrangements are common in cancer and by reporting single
53 breakends the rearrangement landscape of regions previously considered inaccessible to short
54 read sequence can be explored.

55 Short read-based SV detection algorithms identify breakpoints by finding clusters of reads that
56 do not support the reference allele. Typically these use discordant read pairs⁶, or split reads⁷,
57 with some callers also considering reads with unmapped mates⁸ and soft-clipped reads⁹. More
58 sophisticated callers incorporate assembly either through de novo assembly¹⁰, targeted
59 breakpoint assembly¹¹, or breakend assembly¹². These callers report breakpoints, that is,
60 novel adjacencies. When reads cannot be unambiguously mapped on either side, a breakpoint
61 call cannot be made and information is lost. Some callers have attempted to address this by
62 considering multiple alignment locations for each read¹³ but this only works for regions with a
63 small number of potential alignment locations and has proven impractical for general use. Single
64 breakend calling has the potential to improve short read caller sensitivity above the 50%
65 reported in recent benchmarking^{3–5}.

66 As we move closer to a world in which the CNA and SV primitives can be reliably detected,
67 accurate interpretation of the causative biological events becomes increasingly possible by
68 integrated analysis of this knowledge. While progress has been made on derivative
69 chromosome reconstruction using long reads ¹⁴, reconstruction of complex events such as
70 chromothripsis has been problematic for short reads ^{15,16}. To date, SV phasing has been used to
71 reduce the complexity of reconstruction for long read based approaches ¹⁷ but has not been
72 done by short read callers. The ability of phase somatic structural variants is limited by the read
73 length and, for short read data, by the library fragment size - typically less than 500bp.

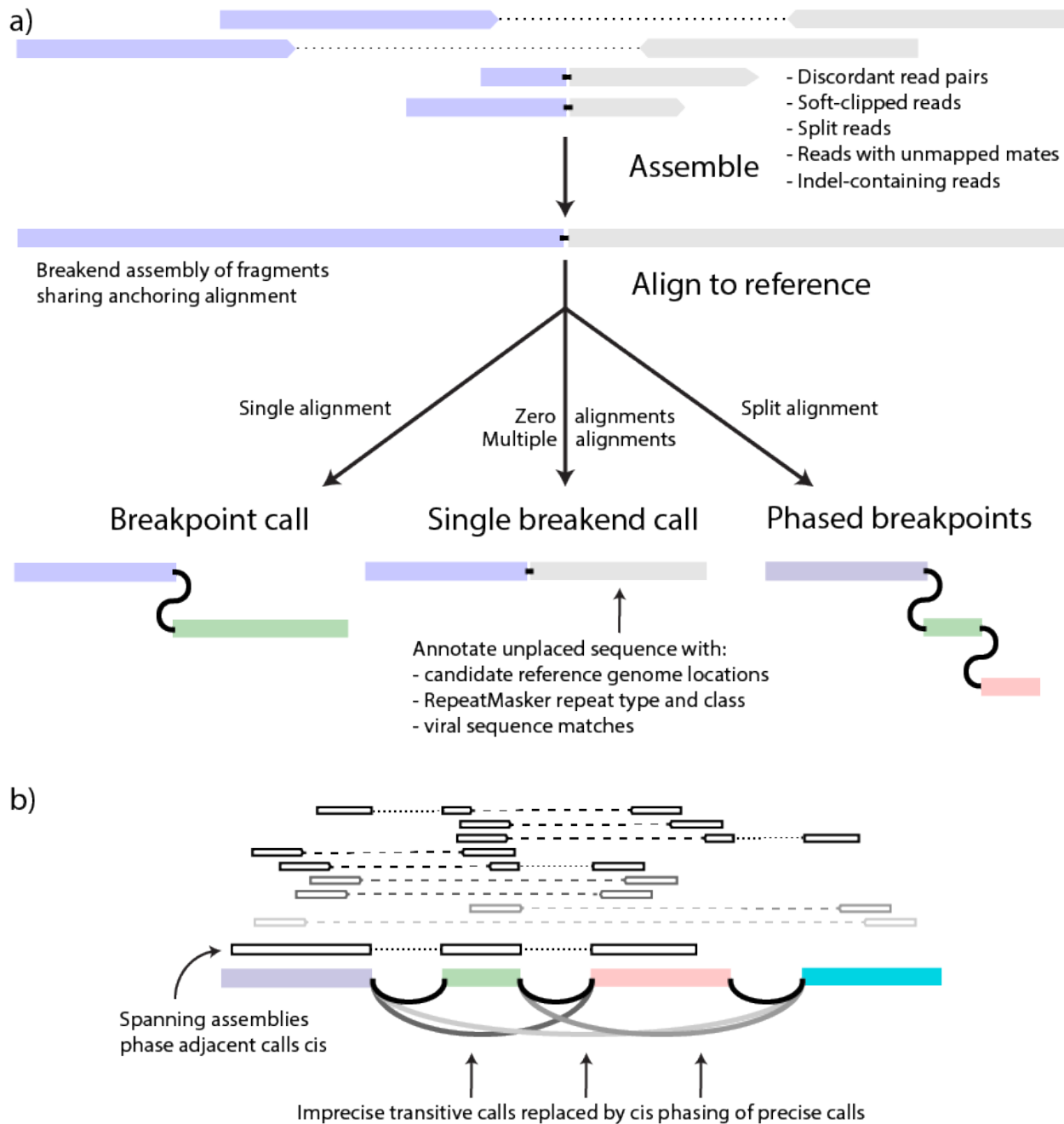
74 Here, we demonstrate the power of single breakend variant calling using GRIDSS2 - a somatic
75 structural variant caller that reports single breakends and phases nearby structural variants.

76 Running GRIDSS2 on 3,782 metastatic solid tumours with matched normal samples from the
77 Hartwig cohort we show that, due to the high prevalence of somatic breakpoints involving low-
78 mappability sequences, GRIDSS2 achieves a false negative rate lower than possible with a
79 traditional breakpoint-only caller. The precision and sensitivity of GRIDSS2 in conjunction with
80 single breakend variant calling and SV phasing lay a strong foundation for downstream tools
81 that enable a deeper understanding of the nature of somatic genomic rearrangements.

82 Results

83 GRIDSS2 utilises the same high-level approach as the first version of GRIDSS, assembling all
84 reads that potentially support a structural variant using a positional de Bruijn graph breakend
85 assembly algorithm¹². Breakend contigs are then realigned back to the reference to identify
86 breakpoints and probabilistic structural variant calling is performed based on both the aligned
87 reads and assembled contigs. Single breakend variant calling uses the same probabilistic
88 variant calling approach as breakpoint calling, but instead of split reads, discordant read pairs,
89 and assembly contigs with chimeric alignments support, single breakends are called based on

90 soft-clipped reads, reads with unmapped or ambiguously mapping mates, and assemblies with
91 unmapped or ambiguously mapping breakend sequence (Figure 1a). SV phasing is performed
92 based on assembly contigs and the presence of transitive calls (Figure 1b). SVs are phased cis
93 if an assembly spans both breaks or a transitive call is found, and phased trans if an assembly
94 involves one SV but supports the reference at the other. Since assembly contig length is limited
95 by the library fragment size only nearby SVs can be phased. GRIDSS2 includes a 16-step
96 somatic filter specifically tuned for deeply sequenced tumour/normal samples.



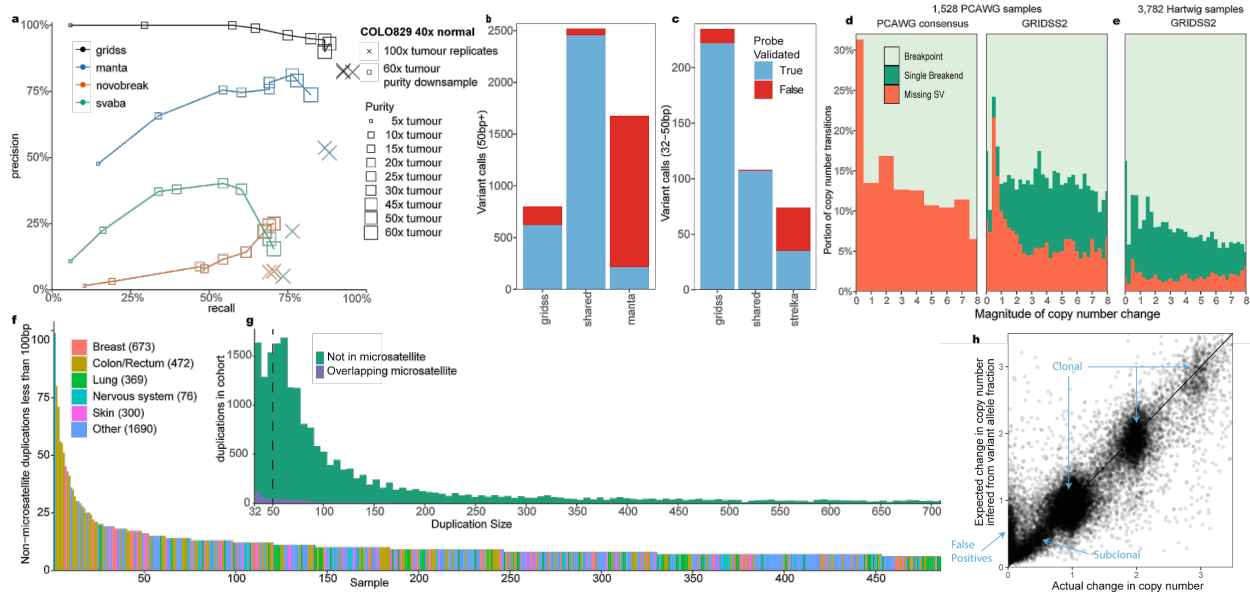
98 Figure 1: GRIDSS2 overview. a) contigs are assembled from a single locus of reads
99 mutually supporting the same putative break junction. If the other side cannot be
100 uniquely determined, the contig supports a single breakend call at the break junction
101 position. If different portions of the contig sequence uniquely align to different genomic
102 loci, the assembly supports multiple cis phased breakpoints. b) Nearby structural
103 variants will have discordant read pairs spanning across multiple breakpoints. These
104 generate spurious transitive calls that are collapsed into the underlying breakpoints,
105 phasing them cis.

106 Benchmarking performance

107 To estimate precision and sensitivity of GRIDSS2, we used a recently generated “gold standard”
108 somatic SV truth set for the COLO829 melanoma cell line and the COLO829BL cell line, which
109 was derived from a normal cell from the same individual, using a combination of Illumina,
110 PacBio, Oxford Nanopore, 10X Genomics linked reads, and optical mapping followed by
111 targeted capture and PCR-based validations and manual curation¹⁸. To test sensitivity and
112 reproducibility, we ran GRIDSS2, Manta¹¹, svaba¹⁹, and novobreak²⁰ on 3 independent
113 sequencing replicates of the COLO829T/COLO829BL matched tumour-normal cell lines
114 sequenced to a depth of 100x tumour and 40x normal coverage. GRIDSS2 achieved an
115 average sensitivity/precision of 94%/83% compared to 88%/52% for Manta, 75%/11% for svaba
116 and 70%/7% for novobreak (Figure 2a).

117 To evaluate performance at lower sequencing depths and sample purity, we use in-silico
118 downsampling and mixing to simulate a matched normal at 40x and a 60x tumour sample at
119 8%-100% purity corresponding to 5x, 10x, 15x, 20x, 25x, 30x, 45x, 50x, and 60x effective
120 tumour coverage. Above 10x effective tumour coverage GRIDSS2 achieved higher sensitivity

121 and specificity than the benchmarked callers. At 10x and below, GRIDSS2 retained higher
 122 precision, but at lower sensitivity than Manta or svaba (Figure 2a).



123

124 Figure 2: Somatic benchmarks. a) COLO829T/BL tumour and blood cell lines were
125 sequenced in triplicate to 100x/40x. In-silico purity downsampling was performed at 40x
126 normal, and 60x tumour coverage. Results are compared against a PCR validated
127 somatic truth set generated from multiple sequencing technologies. b) GRIDSS2/Manta
128 validation results on 13 patient samples for 50bp+ events. c) GRIDSS2/Strelka
129 validation results for 32-50bp events. d) False negative rate (FNR) inferred from the
130 presence of SVs copy number transitions broken down by magnitude of copy number
131 change for 60 PCAWG samples. Comparison is between GRIDSS2/PURPLE and the
132 PCAWG consensus call set. e) Inferred FNR for 3,782 100x tumour samples from the
133 Hartwig cohort. Single breakend variant calling is crucial to the low FNR in this cohort. f)
134 Per sample counts of 32-100bp somatic tandem duplications in the Hartwig cohort.
135 These mutations are enriched in colorectal cancer and associated with ATM driver
136 mutations. g) Size distribution of small (32-100bp) tandem duplications across the
137 Hartwig cohort. This is a distinct signature not associated with microsatellite expansion.
138 h) Comparison of expected vs actual copy number changes for the Hartwig cohort. SV
139 inferred and actual copy number changes are closely correlated.

140 Validation on patient samples

141 To further validate somatic performance, we performed independent validation of GRIDSS2 and
142 manta breakpoint calls from 13 patient tumor samples from the Hartwig cohort ^{2,11,19,20} with a
143 high burden of structural variants. Since the default minimum reported event sizes of GRIDSS2
144 and Manta are 32 and 50bp respectively, we compared 32-50bp events to the short indel caller,
145 Strelka ²¹. We used a hybrid capture approach with target probes flanking and overlapping
146 break-junctions to independently validate over 5,000 calls identified by any tool. 3,403 of 3,666

147 (93%) GRIDSS2 calls were validated compared to 2,685 of 4,299 (65%) for Manta (Figure 2b).
148 Of the private Manta calls not found by GRIDSS2, just 230 of 1777 (13%) were validated
149 compared to 836 of 1031 (81%) GRIDSS2 private calls. Imprecise (that is, not base-pair
150 accurate) Manta calls validated at a rate (40/288, 14%) similar to Manta private calls, whereas
151 GRIDSS2 reports only precise somatic SV. No imprecise GRIDSS2 calls passed somatic
152 filtering, whereas All validated imprecise Manta calls were called by GRIDSS2 precisely. In the
153 32-50bp range, 329 of 343 (96%) of GRIDSS2 calls validated against 142 of 182 (78%) for
154 Strelka (Figure 2c). 95% (219 of 232) of 32-50bp calls private to GRIDSS2 were validated,
155 compared to 47% (35 of 74) for Strelka. Notably, GRIDSS2 finds many short duplications of 32-
156 100 bases which are largely missed by both Strelka and Manta.

157 Novel somatic short duplication signature

158 In addition to reidentifying known kilobase and megabase length duplication signatures, we find
159 a signature consisting of short 32-100bp non-microsatellite tandem duplications (Figure 2f).
160 There is a median of 4 of these short (32-100bp) duplications per sample (Supplementary
161 Figure 1). They are not correlated with larger duplications ($R=0.08$), or total breakpoints
162 ($R=0.10$). Enrichment of samples with 15 or more short duplications is positively associated with
163 colorectal cancer (Figure 2g) ($q=1.2 \times 10^{-9}$) and driver mutations in PARK2 ($q=0.0003$) and ATM
164 ($q=0.008$). Across the Hartwig cohort, 23 samples have driver mutations involving the disruption
165 of a tumour suppressor caused by small duplications.

166

167 These short tandem duplications are too large to be reliably called by most somatic indel callers,
168 but too short to be reliably called by many SV callers. In part this is due to the weak read pair
169 signal due to the short variant length, but also since most callers do not report variants shorter

170 than 50bp threshold used for variant databases such as dbVar. Popular callers such as lumpy²²
171 and delly²³ do not call duplications shorter than 100 and 300bp respectively⁴, and no
172 duplications shorter than 300bp were included in the PCAWG consensus call set¹.

173 Cohort-level FNR/FDR estimation using copy number consistency

174 Structural variant and copy number calls are intrinsically related. Any breakpoint must have
175 either a compensating breakpoint (for example, as with inversions), or a copy number change at
176 that SV position. Using this principle, we can estimate a false negative rate (FNR) from the
177 number of unexplained copy number transitions. To generate matching SV and copy number
178 calls, we ran GRIDSS2 and PURPLE² on 1,528 samples from the PCAWG WGS cohort and
179 compared results with the state-of-the-art PCAWG consensus call set²⁴. Copy number
180 transitions in or within 100kb of centromeres or a gap in the reference genome were excluded.

181 Across the 1,528 samples, GRIDSS2 identified breakpoints for 84% of copy number transitions
182 and single breakends for a further 4.7%, with an estimated 11.2% FNR. The PCAWG
183 consensus call set identified breakpoints for 72% of copy number transitions (28% FNR). When
184 restricted to clonal copy number transitions, the estimated FNR for the PCAWG consensus
185 dropped to 14.2% and GRIDSS2 to 9.36% (Figure 2d), indicating robust subclonal GRIDSS2
186 performance.

187 To evaluate GRIDSS2 on high quality, deeply sequenced samples, GRIDSS2 and PURPLE
188 were run on 3,782 40x normal/100x tumour samples from the Hartwig cohort. Excluding those
189 occurring within 1kb of a gap in the reference genome, 153,231 of 1,954,548 (7.0%) copy
190 number transitions in the Hartwig cohort were explained only by single breakend variants and
191 68,171 (3.1%) lacked a corresponding GRIDSS SV (Figure 2e). The higher rate of single
192 breakend calling can be attributed to GRIDSS2 conservatively calling single breakends and the

193 greater sequencing depth in the Hartwig cohort. The 7.0% of copy number transitions in the
194 Hartwig cohort explained by single breakend variant calls represents a lower bound for the FNR
195 of an exclusively breakpoint-based caller. A FNR of 3.1% suggests that, on this cohort,
196 GRIDSS2 achieves a FNR lower than that possible for a breakpoint-based caller.

197 To demonstrate that this reduction in FNR does not come at the cost of a high false discovery
198 rate (FDR), we compared the change in copy number to the change expected based on the
199 variant allele fraction (VAF). For isolated breaks, the change in copy number should match the
200 variant copy number inferred from the variant allele fraction. Using a 3000bp threshold to ensure
201 at least one full 1kbp copy number bin between SVs, we find that the VAF-inferred SV copy
202 numbers reported by GRIDSS2 are consistent with the copy number changes with no
203 systematic bias in the VAF (Figure 2h). This trend remains true for subclonal variants although
204 the false discovery rate does go up. Assuming variants with a copy number change of less than
205 0.1 and a VAF inferred copy number of at least 0.25 are false positives, GRIDSS2 isolated SV
206 calls have an estimated FDR of 5.4%, with 74% of these subclonal, and single breakends
207 having twice the FDR of breakpoints. Extrapolating these to the rest of the cohort gives an
208 overall estimated FDR of 3.3%.

209 Resolving somatic centromeric rearrangements

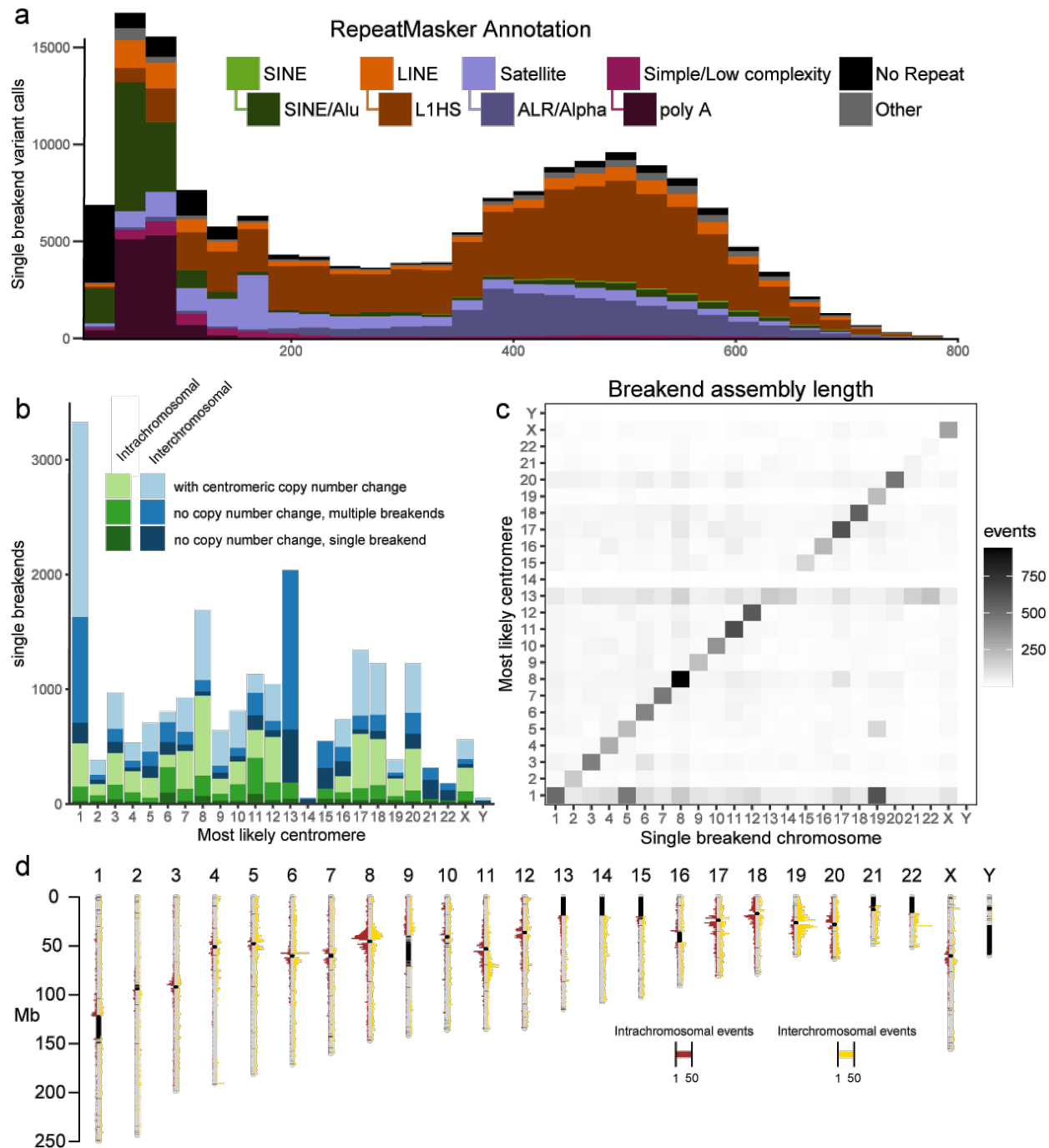
210 Although only one side of single breakend variant calls can be uniquely placed, the assembled
211 sequencing flanking the break can be used to classify integrated provirus, mobile element
212 transposition, rearrangements involving centromeric and telomeric sequence, and other events.
213 RepeatMasker annotation reveals that the majority of somatic single breakend calls are caused
214 by SINE Alu, LINE L1HS insertions or rearrangements involving centromeric sequence, a
215 pattern shared between both the Hartwig and PCAWG cohorts (Figure 3a, Supplementary
216 Figure 2). Breakend assembly lengths for SINE single breakends are typically shorter than

217 150bp as assemblies longer than this can typically be resolved into breakpoint calls. Similarly,
218 the polyA repeat motif characteristic of LINE translocations²⁵ is also found in the shorter
219 breakend assemblies. Such assemblies are short as the de Bruijn graph assembler used
220 truncates assemblies at unresolved repeat loops and assemblies able to span the polyA tail are
221 able to be resolved as breakpoints.

222

223 91% of the Hartwig cohort samples contain at least one copy number transition occurring in
224 centromeric sequence. Being able to resolve the partners of the centromeric breaks explaining
225 these copy number changes is critical to the accurate reconstruction of the derivative
226 chromosomes. Single breakends into ALR/Alpha and HSATII centromeric repeats are able to
227 give significant insight into the nature of these centromeric breaks. As each human centromere
228 has a slightly different dominant repeat sequence, a mapping between each centromeric single
229 breakend and their most likely centromeric breakpoint partner is possible. To do this, we aligned
230 the single breakend sequences containing a centromeric or peri-centromeric repeat against the
231 hg38 reference genome using BLAT, annotating each with the most likely centromeric partner.
232 Using this approach, we were able to explain 5,614 of 11,996 (47%) centromeric copy number
233 changes, implying that approximately half of centromeric rearrangements are centromere to
234 centromere, and the remainder centromere to non-centromeric sequence. Of the 21,587
235 centromeric single breakends detected 3,148 (15%) had no copy centromeric copy number
236 change, 6,850 (32%) had no copy number change but had multiple single breakends linked to
237 the same chromosome, 3,358 (16%) had a single breakend associated with a centromere with
238 copy number change, and the remaining 8,231 (38%) associated with a centromere with copy
239 number change with multiple breakends mapping to that centromere in that sample.

240



242 Figure 3 Classification of single breakends. a) RepeatMasker annotations indicate the
243 majority of somatic single breakends are due to mobile element translocations, or
244 centromeric breaks. b) Most likely centromere for single breakends containing
245 centromeric or peri-centromeric repeats based on realignment of breakend sequence to
246 hg38. Shading indicates whether prediction is consistent with the copy number change
247 across the centromere. Chromosome 1 has an excess of inter-chromosomal breaks to
248 centromeric sequence. Chromosomes 13, 14, 15, 21, 22 have insufficient non-gap p-
249 arm sequence for a centromeric copy number change to be called. c) Location of single
250 breakends to centromeric sequence and corresponding centromere. Chromosome 1
251 has an excess of inter-chromosomal breaks to centromeric sequence, particularly to 5
252 and 19. d) Location of single breakends connected to centromeric sequence on the
253 same chromosome. Red events left of the chromosomes are intra-chromosomal, and
254 yellow events to the right are inter-chromosomal.

255 Novel centromeric break signature

256 The centromeric single breakend rate can be further broken down by chromosome (Figure 3b)
257 and based on the location of the single breakend (Figure 3c). Chromosome 1 is a clear outlier
258 with an overabundance of centromeric inter-chromosomal rearrangements, particularly to
259 chromosomes 5 and 19. Although the high level of sequence similarity between the
260 centromeres of 1, 5, and 19²⁶ could be a cause of false positive predictions, this relationship
261 holds even when restricting the analysis to single breakends with an associated centromeric
262 copy number change (Supplementary Figure 3), implying that the centromeric similarity between
263 1, 5 and 19 results in an increased rate of centromeric rearrangements between these
264 chromosomes. In contrast, the lack of copy number supported single breakends to chromosome

265 13, 14, 15, 21, and 22 centromeres is an artifact caused by missing p arm copy number due to
266 gaps in the reference genome. Similarly, the centromeric sequence homologies between 13, 14,
267 21, and 22 combined with the lack of confirmatory copy number support, make it difficult to
268 determine how much of the high inter-chromosomal centromeric rearrangement of chromosome
269 13 is due to misattribution of rearrangements to other chromosomes.

270

271 In general, intra-chromosomal single breakends to centromeric sequences occur close to the
272 centromere (Figure 3d), with this effect less pronounced for inter-chromosomal breaks.
273 Chromosome 1 is enriched for inter-chromosomal breaks, particularly to chromosomes 5 and
274 19, with inter-chromosomal breaks from these chromosomes to the centromere on 1
275 (Supplementary Figure 4) occurring in a pattern similar to the intra-chromosomal breaks of other
276 chromosomes.

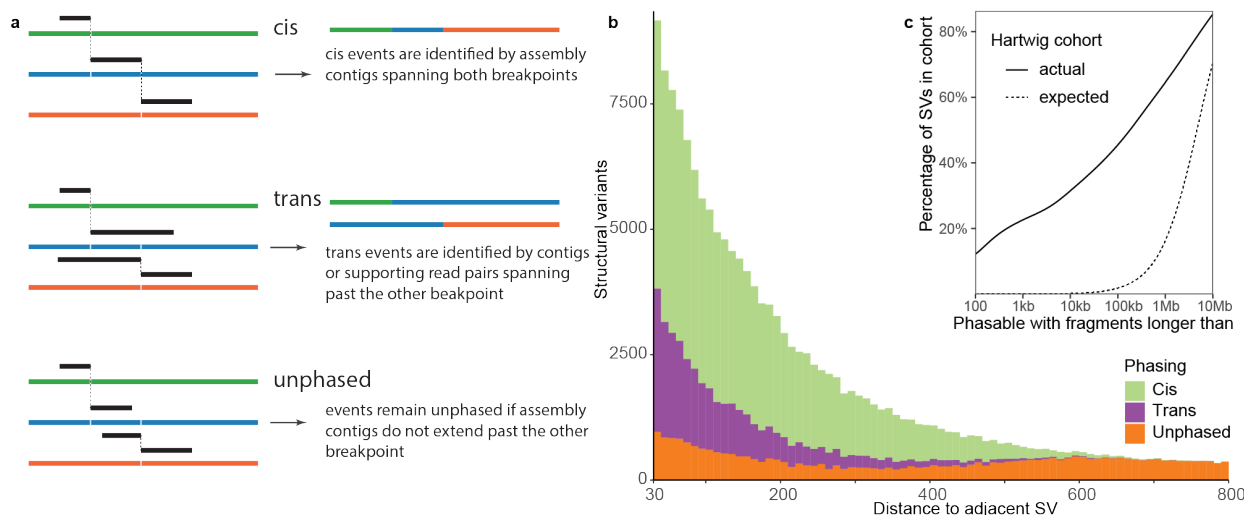
277 Somatic phasing

278 The breakend assembly approach taken by GRIDSS2 also enables the assembly-based
279 phasing of nearby variants. When two structural variants occur in close proximity, they can be
280 phased as cis if the contig aligns across both, and trans if the contig aligning across one aligns
281 to the reference sequence at the other (Figure 4a). Segments shorter than 30bp are not typically
282 uniquely alignable by BWA and unaligned short DNA segments are treated as insert sequences
283 of an SV connecting the longer flanking segments. Since breakend assembly contig lengths are
284 limited by the fragment size distribution of the DNA library sequenced, only nearby variants can
285 be phased.

286

287 For the Hartwig cohort, variants could be phased up to around 500 base pairs. We found that
288 multiple nearby somatic structural variants are frequent, with 22% of all structural variants
289 having an adjacent variant within 1,000bp. This is far in excess of the 0.02% expected if the
290 breakpoints were uniformly randomly distributed (Figure 4c). Of these, GRIDSS2 was able to
291 phase 70% (Figure 4b) with 72% cis and 28% trans. This distribution is recapitulated in the
292 1,528 PCAWG samples and LINX classification of these structural variants indicate that that
293 phasable breakpoint clusters occur predominantly in LINE translocations (due to target site
294 duplication, and highly active donor elements) and highly complex rearrangement events
295 (Supplementary Figure 5). This phasing information greatly assists downstream derivative
296 chromosome reconstruction, as it exponentially reduces the number of possible paths through
297 the breakpoint graph.

298



299

300 Figure 4: Structural variant phasing. a) Phasing of structural variants can be determined
301 when breakend assembly contigs span multiple breakpoints. b) The majority of variants
302 within 600bp can be phased using breakend assembly. c) Somatic SVs are highly
303 clustered with 22% of all SVs in the Hartwig cohort potentially involving a DNA fragment
304 of 1kbp or less.

305 Impact on complex event resolution

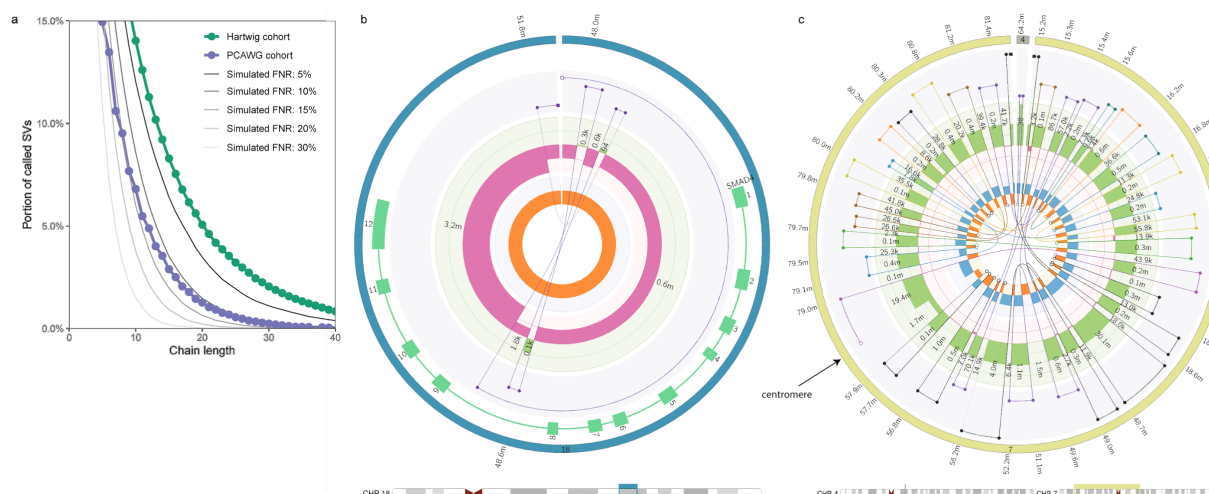
306 To demonstrate the impact on downstream analysis of complex somatic genomic
307 rearrangements, we ran LINX²⁷, a rearrangement event interpretation and classification tool, on
308 the Hartwig and PCAWG cohorts. To fully resolve complex rearrangements structural variants
309 must be chained together to reconstruct the relevant portions of the derivative chromosomes
310 rearranged by the event. If there are errors in the SV call set, it is likely that many complex
311 events will not be able to be fully resolved. To evaluate the impact of FNR on this
312 reconstruction, we evaluated the portion of SVs resolved into long chains for the PCAWG and
313 Hartwig cohorts. In addition, we simulated the effect of increasing FNR by subsampling the
314 Hartwig call set (Figure 5a). 5.0% of SVs in the Hartwig cohort were reconstructed into chains of
315 20 SVs or more. Increasing the FNR reduces this to 3.6% of SVs at 5% FNR, 1.5% at 10%
316 FNR, 0.6% at 15% FNR, and 0.25% at 20% FNR. We previously estimated the PCAWG cohort
317 FNR at 11.2% and we find that the 1.27% of SVs in chains of 20 SVs or more closely match the
318 1.29% we expect from a simulated downsampling of the Hartwig cohort. This implies that the
319 PCAWG and Hartwig pananer cohorts have a broadly similar composition of complex
320 rearrangements and the differences observed are primarily technical in nature. Small
321 improvements in FNR result in large increases in the ability for downstream tools to resolve
322 complex events. A sub-5% FNR is critical for large event reconstruction.

323

324 SV phasing can be critical to the correct interpretation of complex events. For LINX, SV phasing
325 is a critical first step in the chaining of SVs. Of the 486,632 links in the chains resolved by LINX
326 in the Hartwig cohort, 100,007 (21%) were due to GRIDSS2 SV phasing. For the PCAWG
327 cohort, 13,212 of 107,952 links (12%) were resolved by GRIDSS SV phasing, with the
328 difference primarily driven by shallower coverage and shorter library fragment sizes resulting in
329 shorter assembly contig lengths (Supplementary Figure 2), and the higher FNR. In some cases,
330 apparently complex events can be resolved to simple events containing additional short DNA
331 fragments purely through SV phasing (Figure 5b).

332

333 Finally, we use single breakend repeat annotations to identify instances of chromothripsis
334 overlapping centromeres. In the Hartwig cohort, LINX identifies 270 complex events with at least
335 10 breakends to centromeric sequence, 17 of which could be fully chained (Figure 5c). The
336 large number of events with many centromeric single breakends indicates a previously
337 unexplored level of centromeric involvement in complex rearrangements worthy of further
338 investigation.



339

340 Figure 5: Complex rearrangement interpretation. a) Impact of false negative rate (FNR)
341 on complex event resolution. The y-axis indicates the portion of structural variants that
342 form part of a resolved chain of SVs at least as long as the chain length indicated on the
343 x-axis. LINX results for GRIDSS2 calls on the Hartwig and PCAWG cohorts are shown
344 along with simulated results from downsampling the Hartwig cohort to the specified
345 FNRs. A low FNR is essential to accurate complex event resolution. b) Circos plot of
346 SMAD4 driver deletion event. The interpretation of this deletion is confounded by the
347 presence of 3 short fragments at the breakpoint. This event can be fully resolved by
348 GRIDSS2 SV phasing. Circos tracks from innermost to outermost are: single breakends
349 (open white circles) and breakpoints, LOH, copy number, connected segments, genes,
350 chromosome. b) Circos plot of chromothripsis overlapping centromeric sequence. This
351 event spans across the chromosome 7 centromere. A subset of the chromothriptic
352 fragments have been inserted into chromosome 4. Each SV chain is represented in a
353 different colour.

354

355 Discussion

356 Through cell line, patient validation, and cohort-level comparisons, we have shown GRIDSS2
357 has excellent somatic performance above 10x effective tumour coverage. The identification of a
358 small (32-100bp) duplication signature by GRIDSS2 highlights the importance of robust
359 software tested across a wide range of variant types and sizes. The presence of a signature
360 overlapping the widely accepted but arbitrary 50bp threshold separating indels from structural

361 variants suggests it is time to reconsider this threshold as the minimum reported event size for
362 structural variants.

363

364 Explicitly reporting and handling of single breakend variants represents a significant conceptual
365 advancement in the treatment of genomic rearrangements. Even though only the high-
366 mappability side can be unambiguously placed, sequence classification of the low-mappability
367 side produces useful results and meaningful insights. The identification of frequent somatic
368 centromeric rearrangements demonstrates the utility single breakend variant calling has in
369 regions of the genome traditionally considered inaccessible to short read sequencing. Single
370 breakend variant calling provides a framework for the reliable detection of LINE integration
371 without a specialised caller²⁸, for the detection of centromeric and telomeric viral integrations²⁹,
372 and for an entire ecosystem of tools that explicitly model the ambiguity they represent. As single
373 breakends comprise 7.0% of GRIDSS2 calls in the Hartwig cohort, any purely breakpoint-based
374 caller must have a false negative rate of at least 7.0%. GRIDSS2's 3.1% FNR may thus be
375 impossible to achieve for any breakpoint-based caller, at least for this cohort.

376

377 One biologically significant finding coming from GRIDSS2's ability to phase structural variants is
378 the degree to which somatic structural variants are clustered. In the Hartwig cohort of metastatic
379 solid tumours, 22% of somatic structural variants potentially involve DNA fragments of less than
380 1000bp with GRIDSS2 able to phase 70% of these. Long read sequencing is considered the
381 gold standard for structural variant phasing and phasability is indeed better: 10kb long reads
382 increase this theoretical phasability to 31%. The high indel error rate of PacBio and ONT
383 sequencing presents a current drawback of long read sequencing: simple long read based SV
384 detection approaches are likely to misidentify complex rearrangements involving nearby cis-

385 phased SVs. Without HiFi sequencing or error correction prior to alignment, the short DNA
386 segments between the SVs will be unmappable and the long read caller will report a transitive
387 call between the flanking segments as outlined in Figure 1b. On COLO829, we found 5
388 instances (of 67 true positives) in which GRIDSS2 based on short-read sequencing was able to
389 correctly place a short DNA segment that the three long-read callers were not. Care must be
390 taken when comparing or combining short and long read variant calls to ensure the different
391 representations of the same event are reconciled and *cis* phased. GRIDSS2's ability to phase
392 breakpoints involving short DNA fragments is of great utility to downstream rearrangement
393 event classification and karyotype reconstruction as it exponentially reduces the number of
394 possible paths through the breakpoint graph. The highly clustered nature of somatic SVs means
395 that short read sequencing is surprisingly competitive when it comes to phasing somatic
396 variants. Sophisticated analysis and interpretation of somatic genomic rearrangements does not
397 necessarily require long read sequencing.

398

399 Single breakend variant calling enables a sensitivity and specificity unprecedented amongst
400 short read-based somatic structural variant callers, facilitating the resolution of highly complex
401 rearrangements. While breakpoints and copy number segments are widely adopted
402 fundamental genomic rearrangement signals, single breakends have been hitherto unutilised.
403 Their introduction enables the ambiguities present in low mappability regions to be explicitly
404 modelled without compromising FNR or FDR and their potential extends far beyond the
405 examples presented here. GRIDSS2 demonstrates that single breakend variant calling is
406 essential to the comprehensive characterisation of somatic structural variation from short read
407 sequencing data. Combining single breakend variant calling and structural variant phasing with
408 low FNR and FDR, GRIDSS2 represents a foundation upon which sophisticated somatic
409 analysis can be performed.

410 Methods

411 GRIDSS2 extends the GRIDSS¹² software suite with additional features, tools and capabilities.

412 GRIDSS2 is composed of the following 5 phases: (i) preprocessing, (ii) assembly, (iii) variant

413 calling, (iv) annotation, and (v) somatic filtering.

414 Preprocessing

415 GRIDSS2 takes one or more aligned samples in the SAM/BAM³⁰ file format. These files are pre-

416 processed on a per-file basis and all reads supporting a structural variant are extracted, and all

417 fields or tags referring to another record are corrected. Reads with chimeric alignments (i.e. split

418 reads), reads with a soft or hard clipped alignment CIGAR of at least 5bp, read pairs in which

419 only one read is mapped, and discordant read pairs are extracted. The library insert size

420 distribution is estimated from the first 10,000,000 reads using picard tools

421 (<http://broadinstitute.github.io/picard>) and read pairs considered discordant if they fall outside

422 the 99.5% distribution of fragment size lengths. The clipped bases of soft clipped non-chimeric

423 reads are realigned to the reference genome using bwa mem³¹ and converted to a chimeric

424 split read alignments if an alignment is found. Inconsistencies in the mate chromosome and

425 position are corrected (since tools such as GATK indel realignment adjust read alignment

426 positions without updating the mate record), hard clips converted to soft clips, the NM, SA, MC,

427 MQ tags recalculated, and the R2 tag is populated. Improving performance over GRIDSS,

428 GRIDSS2 performs this in a two-pass manner with samtools³⁰ used for name/coordinate sorting

429 the output of the first/second pass respectively.

430 As with GRIDSS, reads with low alignment sequence entropy and reads with a mapping quality

431 (mapq) less than 20 (c.f. mapq<10 GRIDSS) are treated as unmapped, soft-clipped reads with

432 clipped sequence having high homology with standard adapter sequences are ignored, reads

433 marked as duplicates, and regions above 50,000x (c.f. 10,000x) coverage are ignored. Read
434 alignments containing an insertion or deletion under 5bp are considered consistent with the
435 reference.

436 Assembly

437 GRIDSS2 uses the same genome-wide positional de Bruijn graph break-end assembler used by
438 GRIDSS. Reads are split into kmers and associated positions based on the anchoring
439 alignment: kmers from split reads must be assembled only with kmers at the positions inferred
440 by the anchoring alignment, and kmers of unmapped mate reads are assembled at any position
441 consistent with the library fragment size distribution and the anchoring read alignment position.
442 For assembly purpose, split reads and indel alignments are considered multiple soft clipped
443 alignments, and discordant read pairs are treated as multiple read pairs with one read aligned.

444 The output of the assembly is a set of 'soft-clipped' contigs with anchoring bases supporting the
445 reference, and non-reference bases supporting a putative breakpoint at a given position. This
446 contig is iteratively realigned to the reference using bwa mem and converted to a split read
447 alignment. Assemblies longer than the 1.5x maximum fragment size distribution, as well as
448 assemblies supporting the reference sequence are ignored. Assembly alignments with a mapq
449 of less than 20 are treated as unmapped. GRIDSS2 introduces a number of refinements to the
450 assembly calling process.

451 Assembly support is tracked per base pair. Fragments are considered to support a breakpoint
452 only if the fragment support spans at least one base pair beyond any breakpoint homology on
453 both sides. This ensures that when a single contig spans both a germline indel and a somatic
454 SV, the fragments originating from the matched normal sample will not be considered as

455 supporting the somatic breakpoint. This also improves variant allele fraction calculations in
456 regions of complex rearrangement.

457 GRIDSS2 performs compound realignment of the entire assembly contig. BWA is used to align
458 the entire assembly contig. Assembly contig bases which are soft clipped in the primary
459 alignment reported by BWA are fed back to BWA for realignment. This process is repeated until
460 either all bases are aligned, or no alignment can be found for the remaining bases. Assembly
461 contigs that do not overlap with the locus of origin of the assembly are filtered out. To ensure
462 that valid assemblies are not unnecessarily filtered, GRIDSS 2 includes both reads of each
463 fragment in the assembly, and up to 300bp of anchoring reference-supporting sequence is
464 included in the assembled contig. The remaining contigs are treated as split read alignments. To
465 rectify over-alignment of the primary alignment location in the presence of imperfect breakpoint
466 microhomology, the bounds of each split are adjusted to minimise the edit distance to the
467 reference. The originating alignment is tracked using OA SAM tag and contigs that do not
468 partially align to the originating assembly location and strand are filtered.

469 gridss.SoftClippedToSplitReads invokes bwa, -L 0,0 is added to the command line to remove
470 the soft-clipping alignment penalty. This prevents 1bp non-template inserted sequences being
471 over-aligned and reported as clean breakpoints with a flanking SNV.

472 Worse-case assembly performance has been improved by adding an assembly graph path
473 count threshold. Generating 3 assembly contigs with more than 50,000 alternative paths
474 through the assembly graph without advancing the assembly window will flush the assembly
475 window. The maximum assembly window size has been reduced by 2.5x and more aggressive
476 assembly read downsampling in high coverage regions is performed.

477 The presence of a contig with at least three non-overlapping alignments results in the
478 breakpoints supported by that assembly being phased cis. If the initially soft-clipped portion of

479 an assembly realigns across one breakpoint but not another, these breakpoints are phased
480 trans.

481 Variant Calling

482 Breakpoints are called using a probabilistic model based on the empirical distribution of CIGAR
483 operators, the library fragment size distribution, and mapping rate. Each read/read pair is given
484 a phred-scaled quality score based on the mapping quality and the probability of encountering
485 that read/read pair given the library empirical distribution. Split reads and soft clipped reads use
486 the distribution of soft clipping CIGAR operators. Discordant read pairs use the discordant
487 mapping mate if distal or the library fragment size distribution if falling within the range reported
488 by Picard tools CollectInsertSizeMetrics. Reads with unmapped mates use the unmapped mate
489 fragment mapping rate, and indels based on rate of alignments with insertion/deletion CIGAR
490 elements of matching lengths. As with GRIDSS, split reads and breakpoint-supporting
491 assemblies incorporate the mapping quality scores on both sides of the supported break.

492 The key novel feature of the GRIDSS2 variant calling processing is the reporting of single
493 breakend variants. Single breakends variants are called based on supporting soft clipped reads,
494 assembly contigs, and reads with unmapped mates. Single breakend calling uses the same
495 two-pass approach as breakpoint calling with all maximum cliques first calculated, then
496 evidence uniquely assigned to the highest scoring clique.

497 In addition to single breakend variant calling, the variant caller has been improved by: reducing
498 the default minimum called event to 10bp; preferentially allocating reads to variants supported
499 by an assembly containing the read; requiring two supporting fragments to call a variant; and
500 excluding inversion-like breakpoints from the minimum variant size filter to prevent filtering of
501 foldback inversions.

502 Annotation

503 GRIDSS2 provides a full per-sample breakdown of all supporting evidence for each variant

504 through the following VCF INFO and FORMAT fields:

505 • AS, RAS, CAS: counts of assembly contigs supporting a breakpoint originating locally, from
506 the other side of the breakpoint, and from another location respectively. CAS assemblies
507 support multiple variants and provide linking information about those variants.

508 • ASSR, ASRP: total number of split/soft clipped/indel-containing reads, and discordant read
509 pairs/reads with unmapped mate contributing to any breakpoint-supporting assembly contig at
510 the breakpoint location. Note that read/read pairs that are assembled into a contig but whose
511 interval of support does not span the breakpoint are not counted. The interval of support for a
512 read/read pair is defined as the interval between the first and the last contig base for which that
513 read/read pair contributed to the assembly.

514 • SR, RP, IC: counts of split reads and discordantly mapped read pairs, and indel-containing
515 reads that directly support the breakpoint.

516 • BA: counts of assembly contigs support a single breakend at this position. Such contigs are
517 aligned only to the local breakend with the breakend sequence either aligning ambiguously, or
518 unable to be aligned to the reference genome by bwa.

519 • BASSR, BASRP: total number of split reads or soft clipped reads, and discordant read pairs
520 or reads contributing to any breakend-supporting assembly contig at the variant location.

521 • BSC, BUM: counts of soft-clipped reads, and reads with unmapped mates at the variant
522 location

523 • ASQ, RASQ, CASQ, SRQ, RPQ, IQ, BAQ, BSCQ, BUMQ: corresponding quality score
524 contribution for the supporting evidence.

525 • QUAL, BQ: total contribution to the breakpoint/breakend quality score.

526 • BANRP, BANSR, BANRPQ, BANSRQ: counts of read pairs/split reads not supporting this
527 breakpoint but assembled into a contig that supports this breakpoint and their corresponding
528 assembly quality score contribution.

529 • REF/REFPAIR: count of reads/read pairs spanning the local variant position that support the
530 reference allele. Only reads/read pairs that span across the breakpoint microhomology interval
531 (if present) are counted.

532 • VF/BVF: count of unique fragments supporting the breakpoint/breakend. By tracking unique
533 fragments supporting the variant, a more accurate variant allele fraction can be calculated. This
534 approach prevents double-counting of discordantly mapped fragments for which one of the
535 reads contains a split read alignment. A fragment can support a variant either directly through
536 split read, soft clipped read or discordant alignment of a read pair, indirectly through
537 incorporation of one or both of the constituent reads in an assembly supporting the variant, or
538 both directly and indirectly.

539 • RF: count of unique fragments supporting the reference allele.

540 • CQ: variant quality score prior to evidence reallocation.

541 • BEALN: Potential alignment locations of breakend sequence as determined by
542 *gridss.AnnotateInsertedSequence*.

543 • BEID, BEIDL, BEIDH: identifiers of assembly contigs and the corresponding local and
544 remote alignment base offsets. Single breakend variants do not have a remote breakend, and

545 only breakpoint variants include breakpoint-supporting assemblies. Variants containing the
546 same BEID are phased cis.

547 • CIPOS: For IMPRECISE variants, CIPOS encodes the interval in which the breakpoint could
548 occur and for precise variants, CIPOS encodes the homology interval.

549 • CIRPOS: corresponding CIPOS of the remote breakend.

550 • IHOMPOS: interval of inexact homology. A Smith-Waterman alignment of the breakpoint
551 sequence against the reference sequence is performed at both breakends. The reference and
552 breakpoint sequence are extended 300bp from the break on either side with the reference
553 extended an additional 10bp to account for potential indels in the alignment. The homology
554 length is the length that the sequence alignment could be extended from the common sequence
555 into the breakpoint/reference sequence. Alignments containing a soft clip on the common
556 sequence side are classified as alignment errors and ignored. The SSW library³² is used for
557 which we implemented a JNI wrapper. Alignment scored 1, -4, 6, 1 for match, mismatch, gap
558 open, and gap extend respectively which correspond to bwa mem alignment scores.

559 • SC: CIGAR encoding of the anchoring bases that at least one read/read pair/assembly is
560 aligned to and supports the variant. This is encoded as a CIGAR string with a match for each
561 anchoring base that provides support for the variant call, XNX for the interval over which the
562 breakpoint could occur (due to microhomology or an imprecise call), and a deletion CIGAR
563 element for any intervals over which there is no support (such as a small flanking deletion).
564 Variants with an anchoring SC 10bp further from the break than a nearby variant are considered
565 to be phased trans.

566 • SB: Strand bias of the reads supporting the variant. 1 indicates that reads would be aligned
567 to the positive strand if the reference was changed to the variant allele. 0 indicates that reads

568 bases would be aligned to the negative strand if the reference was changed to the variant allele.
569 Strand bias is calculated purely from supporting reads and exclude read pair support since
570 these are intrinsically 100% strand bias. Note that reads both directly supporting the variant and
571 supporting via assembly will be double-counted. Both breakpoint and breakend supporting
572 reads are included.

573 • IMPRECISE, HOMLEN, HOMSEQ, PARID, EVENT, CIEND, END, and SVTYPE fields
574 carry their usual meaning as per the VCF file format specifications.

575 • MQ, MQN, MQX, BMQ, BMQN, BMQX mean, min, and max MAPQ score of
576 reads/assembly contigs providing breakpoint/breakend support.

577 After initial annotation, *gridss.AnnotateInsertedSequence* aligns any single breakend sequences
578 or non-template inserted breakpoint sequences to an arbitrary reference genome and adds an
579 annotation reporting the alignment location. Integrated viral sequence is identified by aligning to
580 a reference of viral sequences. By default, the same reference as the input files were aligned to
581 is used. If a RepeatMasker bed file generated by BedOps³³ rmsk2bed is supplied, inserted
582 sequences will be annotated with the RepeatMasker class and type corresponding to the
583 BEALN alignments.

584 Somatic filtering

585 By default, GRIDSS2 is a sensitive caller and reports all putative variants supported by at least
586 two well-mapped reads. To generate a set of high and low confidence somatic call sets, a
587 somatic filter was developed. Variants with 3% of the supporting reads originating from the
588 normal, or deletion or duplication breakpoints under 1000bp that have any direct split read
589 support in the normal, are hard filtered. Variants are classified as low confidence if any of the
590 following conditions are met: breakend coverage of less than 8 fragments in the normal; allelic

591 fraction of less than 0.5% in the tumour; imprecise variant call; breakend variants without an
592 assembly containing at least one discordant read pair; single breakends with a poly-C or poly-G
593 run of at least 16bp in the breakend sequence; deletion or duplication breakpoints under 1000bp
594 with a split read strand bias of 0.95 or greater; breakpoints with a microhomology of over 50bp;
595 breakpoints with an inexact microhomology of over 50bp which are not deletion or duplications
596 under 1000bp; deletion or duplication breakpoints under 1000bp with no split read support either
597 directly, or through assembly; breakpoints with no discordant read pair support (either directly,
598 or via assembly) which are not deletions or duplications under 1000bp; deletion or duplication
599 breakpoints under 1000bp that have any direct split read support in the normal; 100-800bp
600 deletion breakpoints with an inexact microhomology length of 6bp or greater; inversion-like
601 breakpoints 40bp or less that have at least 6bp of microhomology; deletion-like breakpoints
602 under 1000bp whose length of sequence inserted at the breakpoint is within 5bp of the deletion
603 length, except those whose edit distance to the deleted bases is at least 0.5 per base, and less
604 than 0.2 per base to the reverse complement. Breakpoint variants are filtered if either breakend
605 is filtered.

606 Somatic variants are panel-of-normal (PON) filtered if a match within 2bp was found in a panel
607 of normals. The default hg19 was constructed from the 40x coverage WGS matched normals for
608 3,972 patients from the Hartwig cohort using the *gridss.GeneratePonBedpe* utility. If multiple
609 samples for a patient existed, only the normal for the first sample was included in the PON.
610 Variants were aggregated across samples using the default setting of ignoring the FILTER field,
611 and excluding imprecise calls and breakpoints/single breakends with a QUAL score of less than
612 75/428.

613 Viral insertions are annotated using *gridss.AnnotateInsertedSequence*. Single breakend
614 sequences and non-template inserted sequences that do not have an alignment to the
615 reference genome were aligned to a set of human viral reference sequences. Viral reference

616 sequences were obtained from the virus host database ³⁴ and filtered to include only viruses
617 associated with the homo sapiens taxid of 9606. The viral sequences were then masked using
618 RepeatMasker with “-no_is -s -noint -norna -species human” parameters. Generation scripts can
619 be found at <https://github.com/hartwigmedical/scripts/tree/master/virus>.

620 Assembly linking: pairs of breakpoints mutually supported by a common assembly contig were
621 annotated as linked by assembly. For assembly contigs spanning more than 2 breakpoints,
622 each adjacent pair was linked with a unique identifier to enable unambiguous traversal of the
623 breakpoint graph.

624 Transitive linking: chains of precise breakpoint variants were phased trans if an imprecise
625 spanning transitive breakpoint call could be found. To identify transitive calls, a breadth-first
626 search over the breakpoint graph was performed. Variants were considered transitive if the start
627 and end breakends overlapped the start and end breakpoints in a path of precise breakpoint
628 calls. Paths were limited to 1,000bp and 4 segments, with each segment required to be at least
629 20bp in length. Paths could not self-intersect. To prevent exponential runtime in highly
630 rearranged genomes, at most 100,000 paths and at most 1,000 paths per starting breakpoint
631 were considered.

632 Simple inversion annotation: pairs of breakpoints with orientations consistent with a simple
633 inversion were annotated as simple inversions if the matching breakends were within 35bp on
634 both sides, no other simple event annotation could be applied, and fragments supporting the
635 constituent variants differed by at most threefold.

636 Templatized insertion annotation: breakend/breakpoint and breakend/breakend pairs were
637 annotated as simple templatized insertions if the breakends had opposite orientations, were
638 within 35bp, no other simple event annotation could be applied, and fragments supporting the
639 constituent variants differed by at most threefold.

640 Reciprocal translocation: breakpoint/breakpoint pairs were annotated as reciprocal
641 translocations if the breakends on both sides had opposite orientations, were within 35bp, no
642 other simple event annotation could be applied, and fragments supporting the constituent
643 variants differed by at most threefold.

644 Equivalent: variants were annotated as equivalent if variants had a breakend within 5bp of each
645 other and they shared a common breakend sequence. Breakend sequences were truncated to
646 the length of the shorter sequence and were considered matching when the per-base edit
647 distance between breakend sequences was 0.1 or less. For the purposes of this comparison,
648 the nominal breakend sequence was used for single breakends, and the reference sequence of
649 the partner breakend was used for breakpoint variants. For breakpoint variants, the length of the
650 breakend sequence was the maximum of 20 bases, and the width of the interval over which the
651 fragments supporting the partner breakend had anchoring alignments.

652 Finally, a quality filter was applied to breakpoint variants with a QUAL score of less than 350
653 and single breakend variants with a QUAL score of less than 1000. Variants linked to a variant
654 passing the qual filter other than through equivalence were rescued from the quality filtering and
655 were considered to have passed regardless of the actual variant quality score. For each input
656 file, two output files were generated: a high confidence call set containing calls passing all filters
657 and a low confidence call set containing all calls except those failing the normal support filter or
658 short events with split read support in the normal.

659 Independent validation of SV calls

660 13 samples from the Hartwig metastatic cancer cohort were selected for capture panel
661 validation of the structural variant calls. Each variant called in GRIDSS2 was compared with
662 variants called from Manta (for variants longer than 50 bases) and/or Strelka (for variants from

663 32-50 bases in length) to determine if the variant is shared or private. Variants were marked as
664 matching GRIDSS2 if the start and end chromosomes and orientation both matched and start
665 end positions (including confidence intervals) were within 20 bases of each other. Hybrid capture
666 probes were created for each of the shared and private variants. For each breakpoint variant 3
667 probes of 120 bases each were created: Two reference probes leading up to the breakends
668 from either side, as well as another SV probe going through the structural variant with the break
669 junction close to the middle of the probe. The reference probes were designed to end 20 bases
670 before the start of each structural variant breakend. The SV probe consists of any insert
671 sequence flanked by equal number of bases from each side of the structural variant. For each
672 single breakend variant 2 probes were created: One reference probe as described above and
673 one SV probe which includes no more than 60 bases of the insert sequence with the remainder
674 coming from the reference leading to the break point.

675 Together, this created a total of 17,125 capture probes of 120 nt in length, targeting 5,821
676 break-junctions (see supplementary table 1) which were ordered as custom target capture
677 probes from Twist Biosciences (catalog ID 100533). For each of the 13 samples, 50 ng input
678 DNA was used for indexed library construction with enzymatic fragmentation (Twist kit catalog
679 IDs 100253, 100255 and 100401) according to the manufacturer's protocol. A bead-based size
680 selection was performed after PCR to remove the remaining larger fragments (>700bp).
681 Multiplexed hybridization was performed using the Twist Hybridization (ID100254), Blockers
682 (PN100856) and Wash Kits (PN100214, 100215, 100216)) using Dynabeads™ MyOne™
683 Streptavidin T1 (Invitrogen PN65604D) following standard Twist protocol. Enriched library
684 molecules were amplified by PCR for 11 cycles and sequenced on the Illumina NextSeq500 2x
685 150bp High Output run according to manufacturer's standard protocol.

686 We created a set of predicted alternate contigs from the shared and private structural variant
687 calls using the same technique from above for generating the (non-reference) SV probes and

688 added these to the reference genome. We then mapped each of the reads from the capture
689 panel output with BWA to a hybrid genome including both the GRCH37 reference genome and
690 the novel alternate contig.

691 We assessed the viability of the probes by mapping each of the 120 base SV probes to the
692 2,000 base alternate contigs to determine its mapping quality. Of the 5,821 SV probes, 80 had 0
693 mapping quality and 5,377 had a perfect mapping quality of 60. Probes with a mapping quality
694 of less than 20 were ignored as well as 77 micro-satellite probes that were unable to be
695 unambiguously validated. Resultant BAM files were examined for evidence of the SV alternate
696 contigs in the SV source sample BAM as well as the BAM files of each of the other samples as
697 controls for systemic effects for each of the predicted variants. Specifically, the read depth on
698 the alternate contig at the variant location was used to assess the validation status of the
699 variant. SV calls were marked as validated if all the following criteria were met (and not
700 validated otherwise):

- 701 • At least 2 reads were mapped to the alternate contig in the predicted sample
- 702 • The support rate for the alternate contig was significantly higher (Poisson model, $p=0.001$) in
703 the predicted sample than the maximum of the other 13 samples
- 704 • <40 reads in total across all 13 control samples were mapped to the predicted alternate
705 contig

706 Comparison to PCAWG

707 Copy number data was obtained as for the Hartwig cohort running PURPLE ² with default
708 settings. PCAWG consensus SV and CN calls were obtained from
709 https://dcc.icgc.org/releases/PCAWG/consensus_sv, and

710 https://dcc.icgc.org/releases/PCAWG/consensus_cnv. Copy number transitions were matched
711 with structural variants with a 100kb margin for PCAWG calls, and a 0bp margin for
712 GRIDSS2/PURPLE. Copy number transitions in or within 100kb of centromeres or a gap in the
713 reference genome were excluded from analysis. Copy number transitions matched by both a
714 single breakend and a breakpoint, were considered breakpoint matches.

715 Hartwig metastatic tumour cohort

716 GRIDSS2 was run on 3,782 paired tumour/normal samples from the Hartwig Medical
717 Foundation cohort of metastatic solid cancers with a 32bp minimum event size. Samples were
718 aligned with bwa against a GRCH37 reference genome containing only primary contigs. Single
719 breakend RepeatMasker annotations were obtained by running
720 `gridss.AnnotateInsertedSequence` against the UCSC GRCH37 (hg19) RepeatMasker track
721 downloaded from <http://hgdownload.cse.ucsc.edu/goldenpath/hg19/bigZips/hg19.fa.out.gz> after
722 converting to BED formart using bedops `rmsk2bed`.

723

724 Hartwig copy number was determined by PURPLE. Since PURPLE infers the copy number of
725 short segments by the VAF of the flanking SVs, the copy number of these segments do not
726 represent an independent validation of the SV. As such, FDR was segments from only the
727 breakpoints in which the copy number of all 4 flanking segments was determined of depth of
728 coverage and SNP BAF were considered.

729

730 Single breakends with a RepeatMasker annotation associated with centromeric or
731 pericentromeric repeats were considered centromeric single breakends. The matching

732 chromosome was considered to be the chromosome for which the BLAT³⁵ based score
733 score=(1000-((9-floor(Qsize/100))*mismatch+Qcount+Tcount))*min(match/Qsize,1)) is at least
734 900 and at least 25 higher than the best alignment on a different chromosome when aligning
735 against hg38. A script for annotating likely centromere can be found in
736 example/annotate_most_likely_centromere.R in the GRIDSS repository.

737

738 Phasability of the Hartwig cohort was calculated by determining, for each break junction, the
739 length of the DNA segment if it was phased with the first break junction encountered in the
740 appropriate orientation. Known phasing information was ignored for this analysis. Expected
741 phasability was calculated by simulating 3,782 randomly fragmented paired genomes with the
742 same number of break junctions as the corresponding Hartwig sample.

743

744 For both the PCAWG and Hartwig cohort, rearrangement event classifications were obtained by
745 running LINX²⁸ 1.12 on the GRIDSS/PURPLE outputs. Simulated FNR results were obtained by
746 random subsampling of the Hartwig GRIDS2 SV calls and breaking LINX chains whenever a SV
747 was excluded from the subsampling.

748 COLO829 somatic benchmark

749 The COLO829T/COLO829BL cell lines (ATCC® CRL-1974™ and 1980™ respectively) were
750 each sequenced three times to 100x/40x using the HMF workflow ^{2,4} and aligned against
751 GRCH37 without alt contigs using BWA 0.7.15. GRIDSS 2.9.3, Manta 1.5.0, svaba 1.1.0, and
752 smufin 0.9.3 ³⁶ were run with default parameters. Programs were allocated 8,16,16,20 cores

753 and 32, 32, 50, 500Gb of memory respectively. No smufin results were obtained in any replicate
754 as smufin failed to complete in the 100,000 CPU hours/3 months wall time allocated.

755 Call matching was performed using the StructuralVariantAnnotation BioConductor package
756 (DOI 10.18129/B9.bioc.StructuralVariantAnnotation). A 100bp matching margin was allowed
757 around the break junction position. Tandem duplication calls matched with insertion calls if the
758 size difference between the duplication and insertion was within 25bp. False positive calls under
759 50bp were filtered after matching so as not to penalise a caller reporting an event slightly larger
760 than 50bp in the truth set, but slightly smaller than 50bp in the call set. If multiple calls in a call
761 set matched a single truth set call, all except the highest QUAL call were ignored.

762 COLO829 truth set generation

763 The COLO829 somatic SV truthset was generated using an orthogonal sequencing strategy.
764 We sequenced the COLO829BL and COLO829T cell lines using Illumina HiSeqX (ENA run
765 accessions ERR2752449 and ERR2752450 for COLO829BL and COLO829T, respectively),
766 Oxford Nanopore (ERR2752451 and ERR2752452), Pacific Biosciences (ERR2752447 and
767 ERR2752448) and 10X genomics (ERR2820166 and ERR2820167). All data is grouped under
768 ENA study accession PRJEB27698.

769 Raw data was analysed for structural variants using the following tools:

770 - Illumina data was mapped using BWA 0.7.5, SV calling was performed with GRIDSS 2.0.1
771 and somatic SVs were filtered using gridss_somatic_filter.R.

772 - Nanopore data was mapped using NGMLR 0.2.6 and SV calling was performed with both
773 NanoSV 1.2.0 and Sniffles 1.0.8 separately for COLO829T and COLO829BL. All SVs were

774 merged with an overlap window of 200 base pairs using SURVIVOR 1.0.6 and SVs not present
775 in COLO829BL were kept.

776 - Pacbio data was mapped using minimap2 2.11-r797 and SVs were called using pbsv 2.1.0
777 in joint calling mode for COLO829T and COLO829BL. Only SVs with no evidence in
778 COLO829BL were kept.

779 - 10X genomics data was processed using Longranger 2.2.2 with default settings for
780 COLO829BL and somatic mode for COLO829T. SV calls for both cell lines were merged with an
781 overlap window of 200 base pairs using SURVIVOR 1.0.6 and SVs not present in COLO829BL
782 were kept.

783 Somatic SV calls for each technology were merged with an overlap window of 200 base pairs
784 using SURVIVOR 1.0.6. and all candidate breakpoints were subjected to independent validation
785 by targeted capture and/or PCR-based approaches. SVs detected with two or more techniques
786 that failed in these validation experiments were curated by manual inspection of the mapped
787 reads using IGV³⁷. A total of 69 SVs were finally considered as true somatic SVs for
788 COLO829T.

789 References

790 1. Li, Y. *et al.* Patterns of somatic structural variation in human cancer genomes. *Nature*
791 vol. 578 112–121 (2020).

792 2. Priestley, P. *et al.* Pan-cancer whole-genome analyses of metastatic solid tumours.
793 *Nature* **575**, 210–216 (2019).

794 3. Kosugi, S. *et al.* Comprehensive evaluation of structural variation detection algorithms
795 for whole genome sequencing. *Genome Biol.* **20**, 117 (2019).

796 4. Cameron, D. L., Di Stefano, L. & Papenfuss, A. T. Comprehensive evaluation and
797 characterisation of short read general-purpose structural variant calling software. *Nat. Commun.*
798 **10**, 3240 (2019).

799 5. Danecek, P. *et al.* The variant call format and VCFtools. *Bioinformatics* **27**, 2156–2158
800 (2011).

801 6. Fan, X., Abbott, T. E., Larson, D. & Chen, K. BreakDancer: Identification of Genomic
802 Structural Variation from Paired-End Read Mapping. *Current Protocols in Bioinformatics* 15.6.1–
803 15.6.11 (2014) doi:10.1002/0471250953.bi1506s45.

804 7. Schröder, J. *et al.* Socrates: identification of genomic rearrangements in tumour
805 genomes by re-aligning soft clipped reads. *Bioinformatics* vol. 30 1064–1072 (2014).

806 8. Ye, K., Schulz, M. H., Long, Q., Apweiler, R. & Ning, Z. Pindel: a pattern growth
807 approach to detect break points of large deletions and medium sized insertions from paired-end
808 short reads. *Bioinformatics* vol. 25 2865–2871 (2009).

809 9. Wang, J. *et al.* CREST maps somatic structural variation in cancer genomes with base-
810 pair resolution. *Nat. Methods* **8**, 652–654 (2011).

811 10. Liu, S. *et al.* Discovery, genotyping and characterization of structural variation and novel
812 sequence at single nucleotide resolution from de novo genome assemblies on a population
813 scale. *Gigascience* **4**, 64 (2015).

814 11. Chen, X. *et al.* Manta: rapid detection of structural variants and indels for germline and
815 cancer sequencing applications. *Bioinformatics* **32**, 1220–1222 (2016).

816 12. Cameron, D. L. *et al.* GRIDSS: sensitive and specific genomic rearrangement detection
817 using positional de Bruijn graph assembly. *Genome Res.* **27**, 2050–2060 (2017).

818 13. Sindi, S. S., Onal, S., Peng, L. C., Wu, H.-T. & Raphael, B. J. An integrative probabilistic
819 model for identification of structural variation in sequencing data. *Genome Biol.* **13**, R22 (2012).

820 14. Aganezov, S., Zban, I., Aksenov, V., Alexeev, N. & Schatz, M. C. Recovering rearranged
821 cancer chromosomes from karyotype graphs. *BMC Bioinformatics* **20**, 641 (2019).

822 15. Baca, S. C. *et al.* Punctuated evolution of prostate cancer genomes. *Cell* **153**, 666–677
823 (2013).

824 16. Cortés-Ciriano, I. *et al.* Comprehensive analysis of chromothripsis in 2,658 human
825 cancers using whole-genome sequencing. *Nat. Genet.* **52**, 331–341 (2020).

826 17. Cretu Stancu, M. *et al.* Mapping and phasing of structural variation in patient genomes
827 using nanopore sequencing. *Nat. Commun.* **8**, 1326 (2017).

828 18. Valle-Inclan, J. E., Besselink, N. J. M. & de Bruijn, E. A multi-platform reference for
829 somatic structural variation detection. *bioRxiv* (2020).

830 19. Wala, J. A. *et al.* SvABA: genome-wide detection of structural variants and indels by
831 local assembly. *Genome Res.* **28**, 581–591 (2018).

832 20. Chong, Z. & Chen, K. Structural Variant Breakpoint Detection with novoBreak. *Methods*
833 *Mol. Biol.* **1833**, 129–141 (2018).

834 21. Saunders, C. T. *et al.* Strelka: accurate somatic small-variant calling from sequenced
835 tumor-normal sample pairs. *Bioinformatics* **28**, 1811–1817 (2012).

836 22. Layer, R. M., Chiang, C., Quinlan, A. R. & Hall, I. M. LUMPY: a probabilistic framework
837 for structural variant discovery. *Genome Biol.* **15**, R84 (2014).

838 23. Rausch, T. *et al.* DELLY: structural variant discovery by integrated paired-end and split-
839 read analysis. *Bioinformatics* **28**, i333–i339 (2012).

840 24. ICGC/TCGA Pan-Cancer Analysis of Whole Genomes Consortium. Pan-cancer analysis
841 of whole genomes. *Nature* **578**, 82–93 (2020).

842 25. Tubio, J. M. C. *et al.* Mobile DNA in cancer. Extensive transduction of nonrepetitive DNA
843 mediated by L1 retrotransposition in cancer genomes. *Science* **345**, 1251343 (2014).

844 26. Hayden, K. E. Human centromere genomics: now it's personal. *Chromosome Research*
845 vol. 20 621–633 (2012).

846 27. Cameron, D. L., Baber, J., Shale, C. & Papenfuss, A. T. GRIDSS, PURPLE, LINX:
847 Unscrambling the tumor genome via integrated analysis of structural variation and copy number.
848 *bioRxiv* (2019).

849 28. C Shale, J Baber, DL Cameron, M Wong, MJ Cowley, AT Papenfuss, E Cuppen, P
850 Priestley. Unscrambling cancer genomes via integrated analysis of structural variation and copy
851 number. *bioRxiv* (2020).

852 29. Cameron, D. L. & Papenfuss, A. T. VIRUSBreakend: Viral Integration Recognition Using
853 Single Breakends. doi:10.1101/2020.12.09.418731.

854 30. Li, H. *et al.* The Sequence Alignment/Map format and SAMtools. *Bioinformatics* **25**,
855 2078–2079 (2009).

856 31. Li, H. & Durbin, R. Fast and accurate long-read alignment with Burrows-Wheeler
857 transform. *Bioinformatics* **26**, 589–595 (2010).

858 32. Zhao, M., Lee, W.-P., Garrison, E. P. & Marth, G. T. SSW library: an SIMD Smith-
859 Waterman C/C++ library for use in genomic applications. *PLoS One* **8**, e82138 (2013).

860 33. Neph, S. *et al.* BEDOPS: high-performance genomic feature operations. *Bioinformatics*
861 **28**, 1919–1920 (2012).

862 34. Mihara, T. *et al.* Linking Virus Genomes with Host Taxonomy. *Viruses* **8**, 66 (2016).

863 35. Kent, W. J. BLAT--the BLAST-like alignment tool. *Genome Res.* **12**, 656–664 (2002).

864 36. Moncunill, V. *et al.* Comprehensive characterization of complex structural variations in
865 cancer by directly comparing genome sequence reads. *Nat. Biotechnol.* **32**, 1106–1112 (2014).

866 37. Robinson, J. T. *et al.* Integrative genomics viewer. *Nature Biotechnology* vol. 29 24–26
867 (2011).

868 38. Zook, J. M. *et al.* A robust benchmark for detection of germline large deletions and
869 insertions. *Nat. Biotechnol.* (2020) doi:10.1038/s41587-020-0538-8.

870 39. Wang, Q., Jia, P. & Zhao, Z. VirusFinder: software for efficient and accurate detection of
871 viruses and their integration sites in host genomes through next generation sequencing data.
872 *PLoS One* **8**, e64465 (2013).

873 **Acknowledgements**

874 S. E. de Garis for manuscript feedback and copyediting.

875 This publication and the underlying study have been made possible partly on the basis of the
876 data that Hartwig Medical Foundation and the Center of Personalised Cancer Treatment
877 (CPCT) have made available to the study.

878

879 Author Contributions

880 DLC designed and implemented GRIDSS2. DLC, PP, JB, CS designed and performed dry lab
881 experiments and analysis. JEV provided COLO829 golden reference data. NB performed
882 independent break junction validation experiments. AH, RJ generated the
883 GRIDSS2/PURPLE/LINX TCGA call set. ATP, PP, EC designed and supervised experiments.
884 DLC, ATP, PP, EC contributed to writing of the manuscript.

885 Competing Interests

886 The authors declare no competing financial interests.

887 Availability of data and materials

888 GRIDSS2 source code is available as free and open source software from
889 <https://github.com/PapenfussLab/gridss> under a GPLv3 license. GRIDSS2 releases are
890 available as a github release, bioconda package, and docker image. Analysis scripts used to
891 generate results are available from
892 https://github.com/PapenfussLab/gridss/tree/master/scripts/gridss2_manuscript.

893

894 Hartwig cohort data was obtained from the Hartwig Medical Foundation (Data request DR-005).
895 Standardized procedures and request forms for access to this data can be found at
896 <https://www.hartwigmedicalfoundation.nl/en>.

897

898 Raw and analyzed data for the creation of the COLO829T/COLO829BL tumor/normal cell line

899 pair structural variant truth set are available grouped under ENA study accession PRJEB27698.

900 The COLO829 truth VCF is available from

901 https://github.com/UMCUGenetics/COLO829_somaticSV.

902

903 Capture panel validations of 13 patient tumor samples are available under the controlled access

904 dataset accession EGAD00001005525.

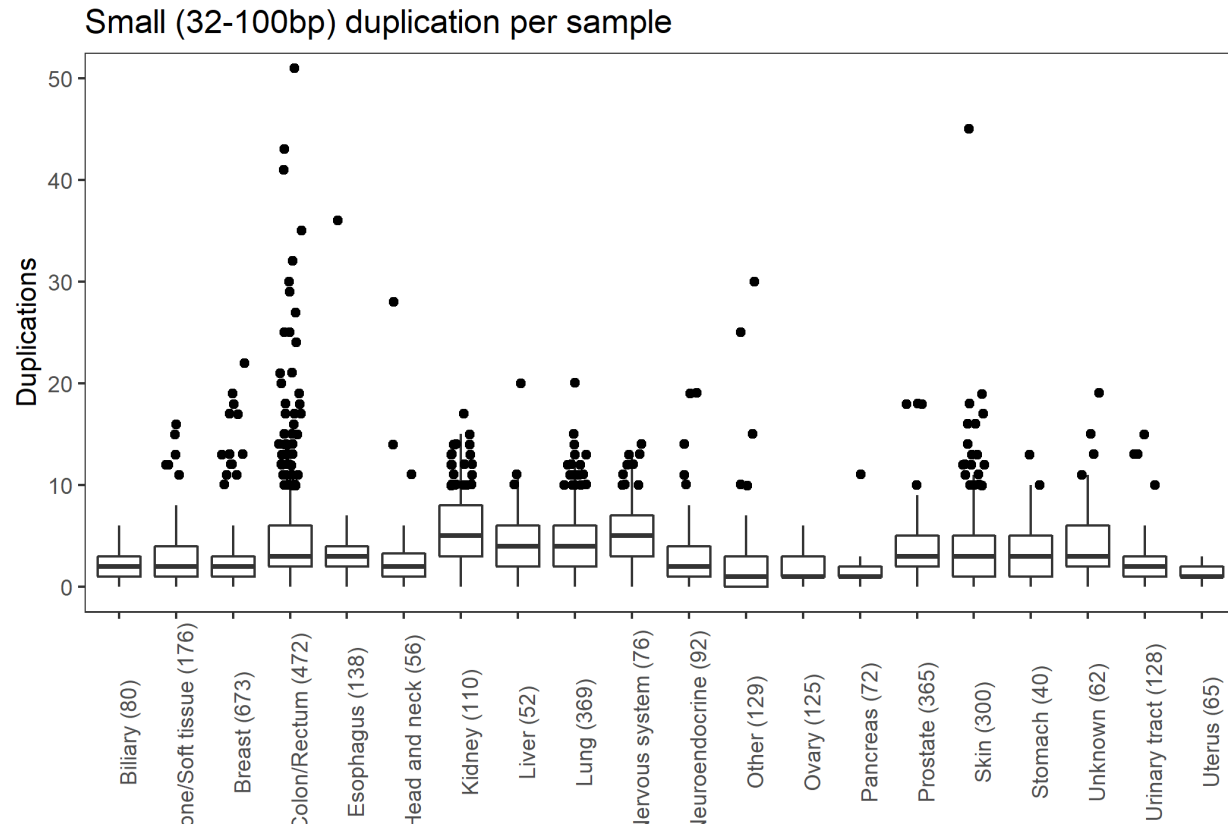
905

906

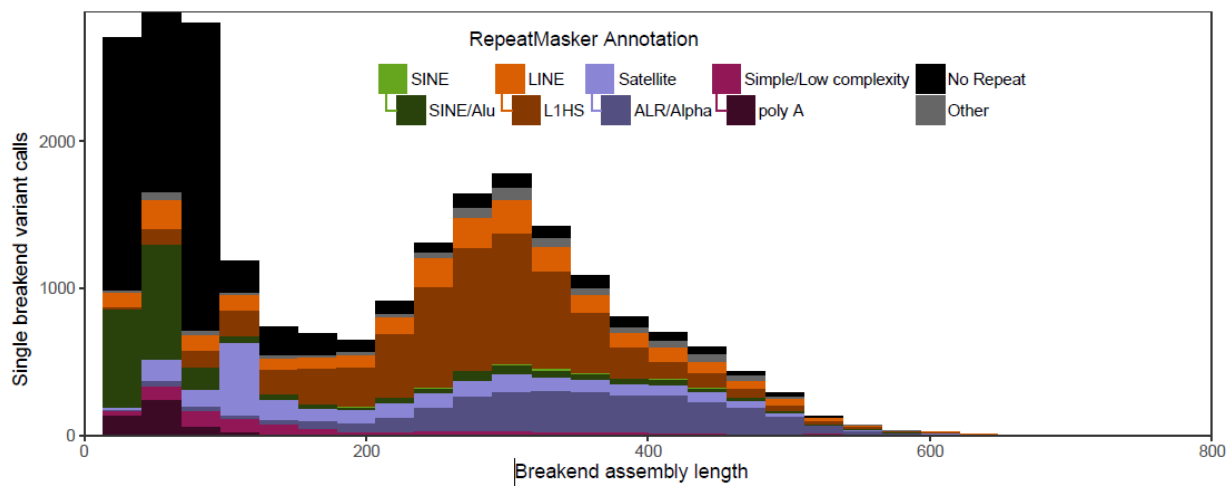
Supplementary Figures

907 Supplementary Figure 1: Distribution of 32-100bp duplication events per cancer type.

908



909

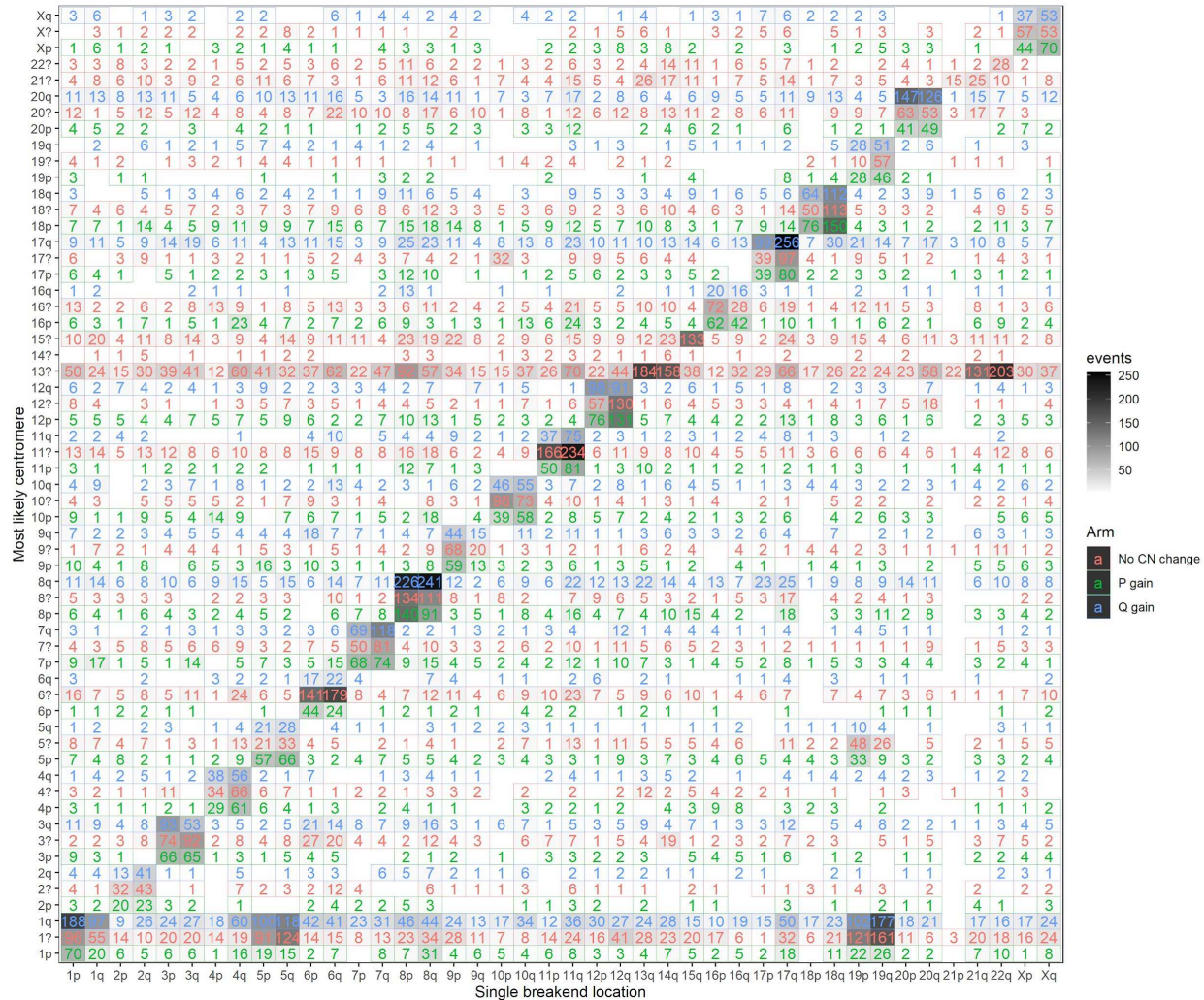


910

911 Supplementary Figure 2: Single breakend RepeatMasker annotation for 1,528 PCAWG
912 samples.

913

914

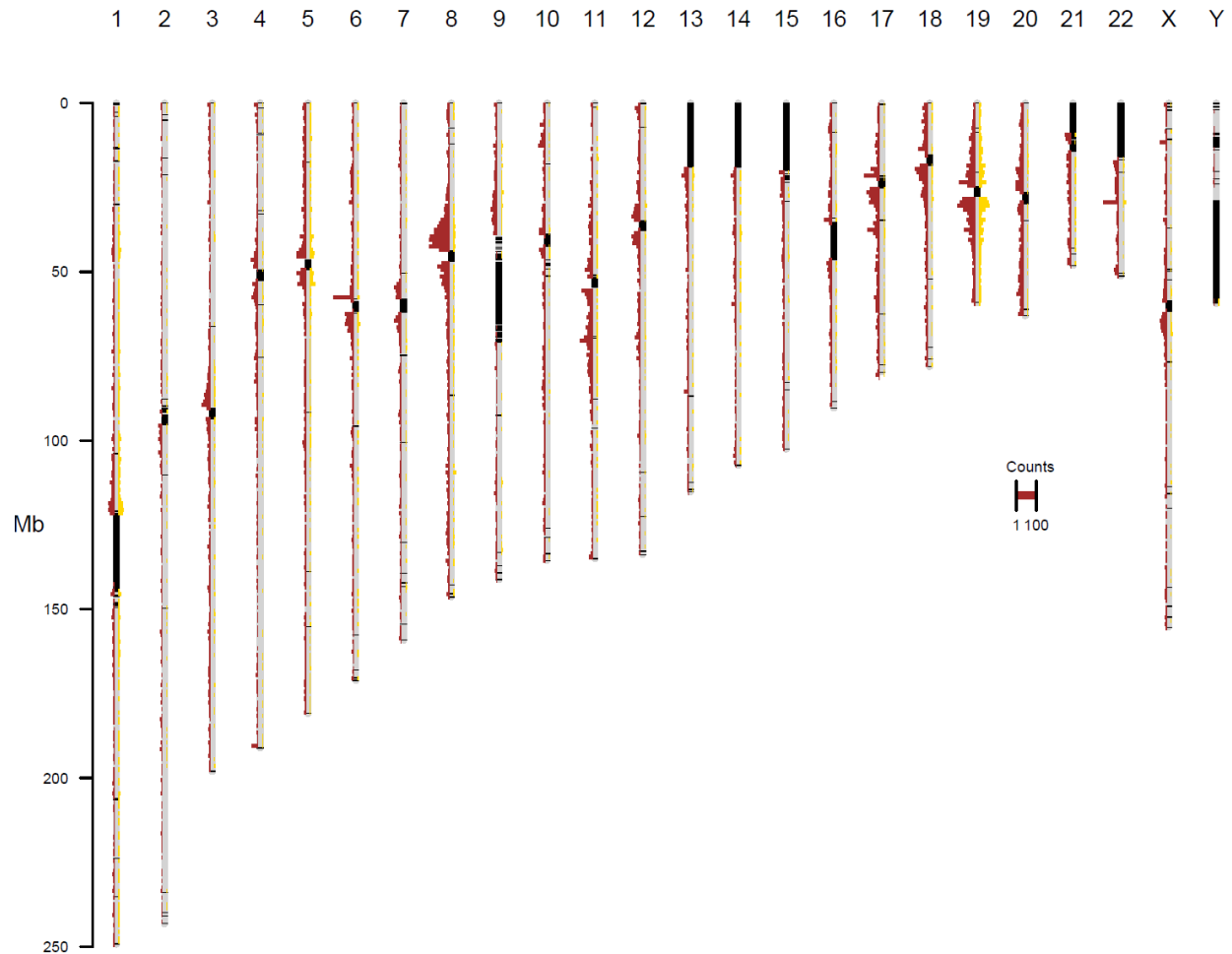


915

916 Supplementary Figure 3: Heatmap of single breakends to centromeric sequence by
 917 chromosomal arm. The x axis indicates the arm of the single breakend with the y axis indicating
 918 the most likely chromosomal arm the single breakend is connected to based on the breakend
 919 sequence, and the copy number profile across the centromere. ? indicates the arm is unknown
 920 due to the lack of copy number change across the centromere, and p and q indicate a
 921 centromeric copy number gain to that arm.

922

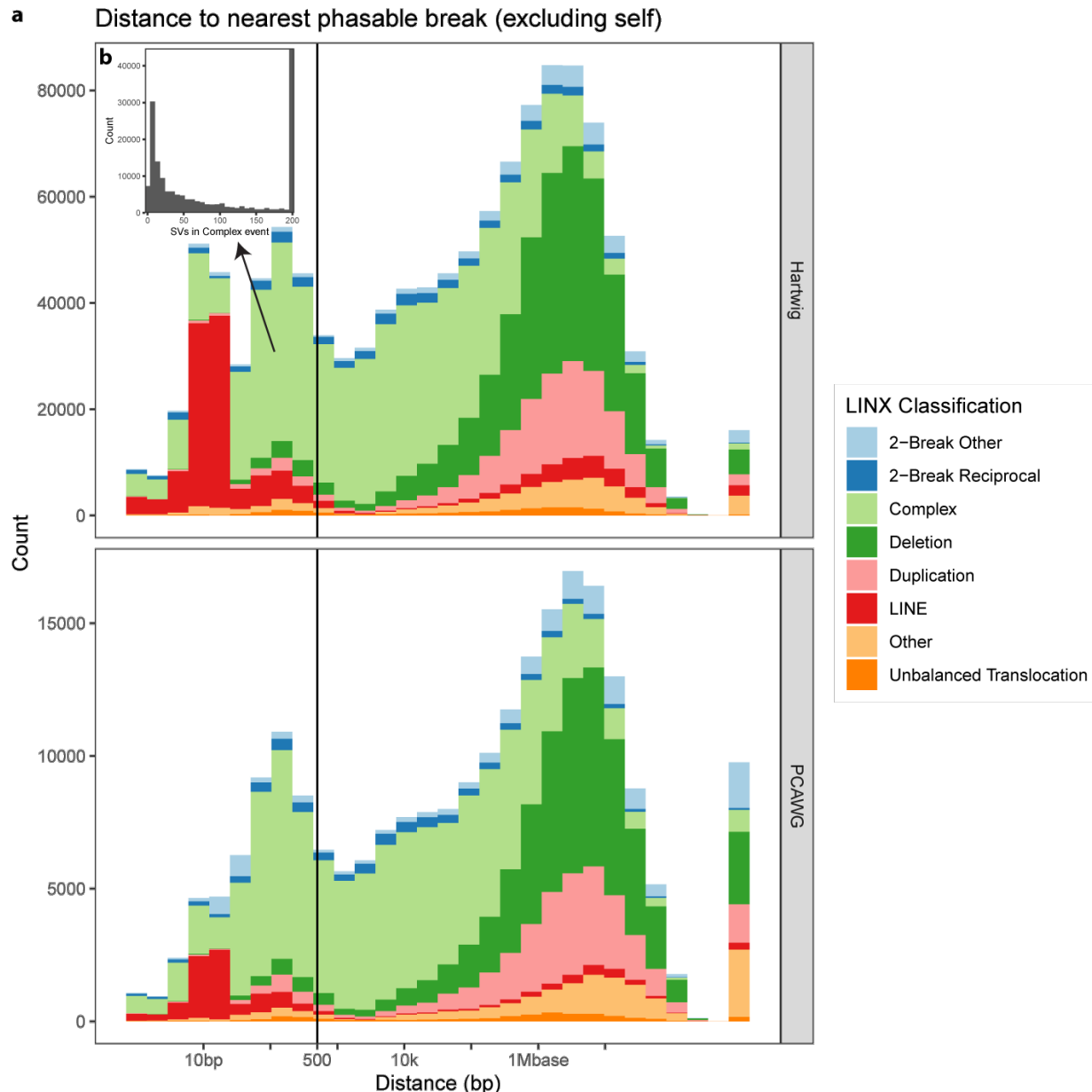
923



924

925 Supplementary Figure 4: location of single breakends associated with the chromosome 1
926 centromere. Red indicates a single breakend associated with centromeric sequence on the
927 same chromosome, yellow indicates a single breakend associated with centromeric sequence
928 on chromosome 1. Single breakends to chromosome 1 occurring on chromosomes 5 and 19
929 follow a similar distribution to intra-chromosomal single breakends.

930



931

932 Supplementary Figure 5: a) Phasability and LINX classification of structural variants in the
933 Hartwig and PCAWG cohorts. Phasable variants are predominantly LINE translocation or form
934 part of complex events. b) Number of SVs in complex event clusters containing phasable SVs.
935 Most phasable SVs occur in highly complex events.